CONCRETE LIBRARY OF JSCE NO. 28, DECEMBER 1996

BEHAVIOR OF EMBEDDED BARS IN CONCRETE UNDER COMBINED AXIAL PULLOUT AND TRANSVERSE DISPLACEMENT

(Reprinted from Journal of Materials, Concrete Structures and Pavements, No. 532, V-30, 1996)

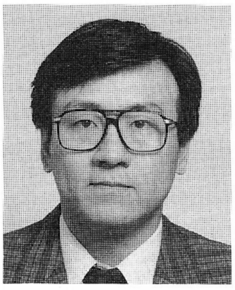

Koichi MAEKAWA

Juneid QURESHI

This paper investigates the pullout behavior of embedded deformed bars in concrete under coupled transverse shear arising at cracks in reinforced concrete. It is experimentally proven that when the pullout capacity -- achieved when steel section yields at a crack under uniaxial tension -- is reached, full yielding of steel bars is not observed in the critical section where the axial stress is maximum. The ultimate limit state is attained not at the RC crack plane but at the location where induced curvature by shear slip of crack takes place. It is concluded that under higher reinforcement ratio and/or flatter planes of concrete joints, coupling of pullout and transverse shear of steel at a crack cannot be ignored in structural analysis.

Keywords*: Dowel action, bond, crack, reinforcement, joint interface*

K. Maekawa is a Professor in the Department of Civil Engineering at the University of Tokyo. His research interests cover reinforced concrete mechanics, computational approaches to the seismic behavior of reinforced concrete-soil systems, the thermodynamics of cement-concrete composites and the durability design of concrete structures.

J. Qureshi is an Assistant Professor in the Department of Civil Engineering at NED University of Engineering and Technology, Karachi, Pakistan. His research interests cover reinforced concrete mechanics and steel-concrete composite. He earned his doctoral degree from the University of Tokyo in 1993.

---

1. INTRODUCTION

Recent developments in predicting structural concrete behavior have been achieved by enhancing the constitutive laws for reinforced concrete[1]. Among the enhanced constitutive laws, bond behavior is of primary importance since the major nonlinearity of RC members originates from crack planes reinforced by deformed bars. The macroscopic aspects of bonding are conventionally modeled in terms of tension stiffening of the concrete or pullout of discrete embedded bars from concrete[2]. These computational models have been applied to both discrete and smeared crack elements in the frame of nonlinear finite element analysis[1].

In general, bar stress in crack planes is computed only with respect to pullout slip geometrically defined *along the axis of the bars*. The presence of displacement perpendicular to the axis of the bars is not taken into account in computing axial stress-pullout relations, and the applicability of this method, which offers simplicity of computation, has been carefully examined by Mishima et al[4]. Through their experimental verifications, it was clarified that reinforced concrete normal cracks, which are introduced by tensile stress in the concrete and reinforced by deformed bars with reinforcement ratio not greater than 2%, can be successfully dealt with by the simple superposition of stress transfers in concrete crack[11] and the bond-slip model of a single reinforcing bar [2].

However, it became simultaneously manifest that this simple superposition leads to overestimated shear capacity of the reinforced concrete crack planes and higher than actual shear stiffness when the reinforcement ratio is greater[5]. Along with recent developments in enhanced micro-mechanical constitutive modeling[11],[12], this tendency has been getting more and more clear. For heavily reinforced crack and/or joint planes with a smoother surface configuration, the reduction in confinement efficiency as a result of reinforcing bars crossing shear planes has become an issue owing to coupled displacement paths consisting of transverse displacements and axial pullout [5],[13].

At present, no convincing experimental proof of heavily reinforced crack that is also adaptable to computational models has been supplied. This paper deals with the behavior of embedded deformed reinforcing bars under coupled interface opening and transverse shear displacement, and both macro- and micro-mechanical aspects are carefully discussed. The main focus is on the axial mechanical performance of an embedded reinforcing bar under the presence of coupled dowel action on the bar. In this study, the reinforcing bar is treated not as a one-dimensional cord but as a three-dimensional body.

2. PULLOUT TESTS ON EMBEDDED BAR UNDER COUPLED TRANSVERSE SHEAR

(1) Specimens and loading

The coupled pullout and transverse shear displacement paths were introduced to a reinforcing bar at a crack by applying pure shear loading on a beam-type specimen as shown schematically in **Fig.1**. The interface opening denoted by ω_s was measured at two places on each face of the specimen, and the transverse displacement defined as δ was measured at mid-depth on each face. The pullout (denoted by S and defined as bar axial displacement measured based on concrete point of far field[2]) at the center of the interface section was measured with a gap sensor directly through a stainless steel wire inserted in a plastic tube as shown in **Fig.1**. Here, the far field point was set at the concrete surface on which the gap sensor was attached.

The plastic tube was attached to the bar at several locations and wax was applied along its length to ensure debonding with the concrete and free movement of the tube when the bar undergoes transverse displacement. The sectional stress of a reinforcing bar at the interface where shear slip was induced was obtained by measuring the strain and using a predefined stress-strain relation for the bar concerned. The embedded length of the bar was at least 25D (where D denotes bar diameter) so that sufficient anchorage was guaranteed and the free end slip of the bar is negligible[2]. The specimens were loaded monotonically to failure. Details of specimen dimensions, mechanical properties, bar arrangement, material properties, and interface types are listed in **Table 1**.

The test set-up and loading arrangement chosen for this study have inherent advantages and disadvantages. As shown in **Fig.2(a)**, another possible set-up would be to directly apply axial load P and transverse shear V to a bar. The advantage in this case is that any type of load history could be controlled.

Table 1 Dimensions, mechanical and material properties, and types of interfaces for specimens tested

Specimen	b*h(mm)	p (%)	fy (MPa)	D (mm) center	D (mm) side	fc' (MPa)	Concrete type	Joint type
1	150*300	1.18	446	25	none	40	NC	RC
2	200*300	2.24	446	25	16(4bars)	41	NC	RC
3	200*300	4.44	403	25	25(4bars)	48	NC	RC
4	150*300	1.57	480	25	none	40	HPC	U-CJ
5	150*200	0.95	450	13	13(2bars)	35	HPC	U-CJ
6	150*200	1.58	450	13	13(4bars)	35	HPC	U-CJ
7	150*150	1.84	360	16	16(1-bar)	50	HPC	P-CJ
8	150*150	0.95	360	16	none	43	HPC	U-CJ
9	150*150	0.95	360	16	none	42	HPC	P-CJ
10	150*150	0.95	360	16	none	27	NC	U-CJ
11	150*150	0.95	360	16	none	28	NC	P-CJ

/b*h : width and height of the section /p : reinforcement ratio /fy : yield strength of the bars /fc' : compressive strength of concrete
/Specimens 4, 5, 6, and 7 are instrumented with strain gages along their axis; all other specimens instrumented with strain gages only at the interface.
/Bar arrangement is symmetric in cross section for all specimens as illustrated in Fig.3.
/NC : normal concrete /HPC: self-compacting concrete /U : unprocessed /P : tipping process /RC : rough crack /CJ : construction joint

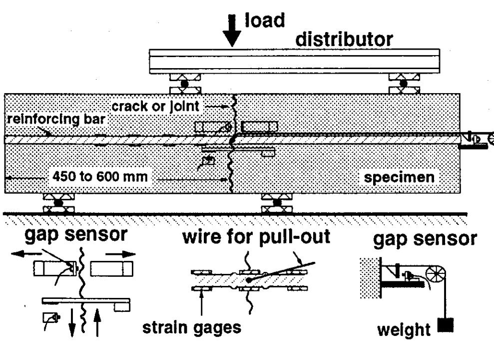

Fig.1 Test set-up and instrumentation

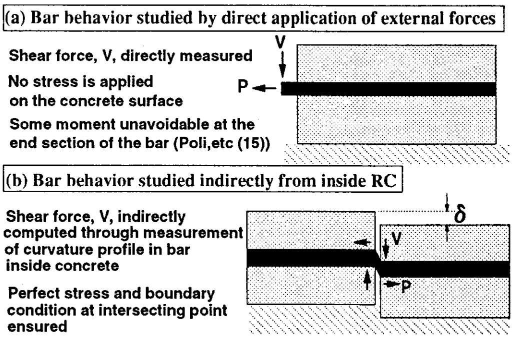

Fig.2 Schematic arrangement for investigating embedded bar behavior

On the contrary, it would be difficult to reproduce real boundary conditions. The bending moment on the bars must be zero at the interface, but this could not be guaranteed here. In fact, compressive confining stress acts on the rough crack surface around the bars owing to the shear dilatancy mechanism; however, method (a) in **Fig.2** produces perfectly zero confinement.

Concerning the approach chosen in this study, although it is impossible to either obtain the transverse force directly or freely control the load paths, a perfect boundary condition is ensured at the intersecting point. The aim of this approach is to pick up information from within the reinforced concrete on the embedded bar in as stable a manner as possible. Also, the transverse force carried by the bar, although not directly measured, can be computed provided that the associated bending moment along the bar axis is known, as discussed in later section.

The tension applied to the bar originates from interface dilatancy associated with the transverse shear. The important point is that the bar at the interface is subjected to the general condition of coupled pullout and transverse displacement as measured along the interface. The axial force induced in the bar is controlled by intentionally changing the geometrical profile of the crack plane as well as by placing additional reinforcement around the target bar, thereby changing the reinforcement ratio.

A rough crack, which makes the crack gap wider, is introduced by splitting tension force and the associated roughness is generated. A flat plane, which induces smaller interface opening coupled with shear slip, is also reproduced by constructing concrete on the surface of a previously cast concrete construction joint. By this method, successful reproduction of different pullouts, denoted by S ($\cong\omega_s/2$), versus transverse shear ($=\delta/2$) paths of the embedded bar at the interface were experimentally simulated over a wide range.

(2) Pullout affected by transverse shear

The pullout slip versus mean axial stress for typical specimens at the interfaces is shown in **Fig.3**. Notations in these figures are the same as those defined in **Table 1**. The uniaxial pullout behavior, obtained under axial force only and predicted fairly by the model of Shima et al.[2], is also shown for reference in **Fig.3**. Under pure axial pullout, the pullout stiffness is close to zero when reinforcing bar stress at the crack reaches the yield strength of the bar, because the plastic range penetrates from the crack point into the section of steel inside the concrete. As reported by Mishima et al.[7], this common pullout behavior can be seen even under coupled displacement paths of axial pullout with transverse shear along a crack.

However, the pullout stiffness is reduced even when the axial stress is lower than the yield strength, as shown in **Fig.3**. The point where this fall in stiffness initiates is directly influenced by the field of the induced displacement path. Higher ratios of transverse displacement to axial pullout induce earlier initiation of the deviation from the pure axial pullout stiffness, as can be seen in **Fig.3(a,c)**. Also, the maximum confining stress provided by embedded bars at a crack section, $\sigma_{s,ult}$, which determines the ultimate shear capacity, is much less than the uniaxial capacity of bare steel bars represented by f_y.

At the crack section, the steel was found to be still elastic despite the inelastic pullout from the concrete. When the crack opening was confined more by additional reinforcement, a significant reduction in anchorage performance represented by $\sigma_{s,ult}$ was detected. But the elasticity of the steel at the crack section was verified. The reduction in mean yield strength, defined as the axial capacity under coupled shear and pullout from the uniaxial yield strength of the steel, varied from 22% for lightly reinforced sections, Specimen 1 (p=1.2%, with one 25mm diameter bar), to as much as 67% for heavily reinforced sections, Specimen 3 (p=4.4%, with five 25mm diameter bars), as seen in **Fig.3(a,c).**

This reduction was also checked by changing the displacement paths. Some specimens were tested with crack planes designed as a construction joint, as explained earlier. Smooth crack asperity, and the resultant high ratio of transverse displacement to crack opening was associated with a more significant reduction in mean yield strength of the bar, even at low reinforcement ratios, with a reduction of about 39% for Specimen 5 (p=0.95%, with three 13mm diameter bars) and about 47% for Specimen 6 (p=1.58%, with five 13mm diameter bars) as shown in **Fig.3(e,f)**. Specimen 5 exhibits a larger reduction than Specimen 1, even though the reinforcement ratio is smaller. This is thought to be caused by the smoother interface.

In the case of Specimen 10 with an unprocessed construction joint of normal concrete, a very steep displacement path in terms of bar transverse displacement to axial pullout is observed, and the mean yield strength is reduced by as much as 56% even though p is only 0.95% as shown in **Fig.3(h).**

From these results, it can be concluded that the pullout behavior deviates from that obtained under pure axial tension, which has been the broad focus of attention in past research[8]. Furthermore, the higher the ratio of transverse displacement to crack opening -- achieved by higher reinforcement ratio, flatter interface surface geometry, or lower concrete strength -- the lower the capacity of the anchorage. In the past, the shear failure of concrete crack planes has been reported [14] as the counterpart of yielding failure of reinforcement at a crack. According to reduced axial stiffness and steel confinement, the shear failure mode, which was supposed to be associated with the failure of the crack plane, needs to be re-examined in detail.

3. MECHANISM OF REDUCED AXIAL PERFORMANCE UNDER COUPLED SHEAR

(1) Local yield of steel inside concrete

Since a flatter plane with less dilatancy results in a considerable reduction in pullout stiffness, the microscopic mechanism associated with this reduced stiffness and capacity was investigated as shown in **Fig.4**. Since the reduced of pullout resistance must be rooted in local plasticity arising in the embedded steel bars, profiles of local curvature and mean axial strain were locally measured. Grooved bars were utilized to enable the attachment of strain gages while maintaining local bonding. Measurements were taken along the

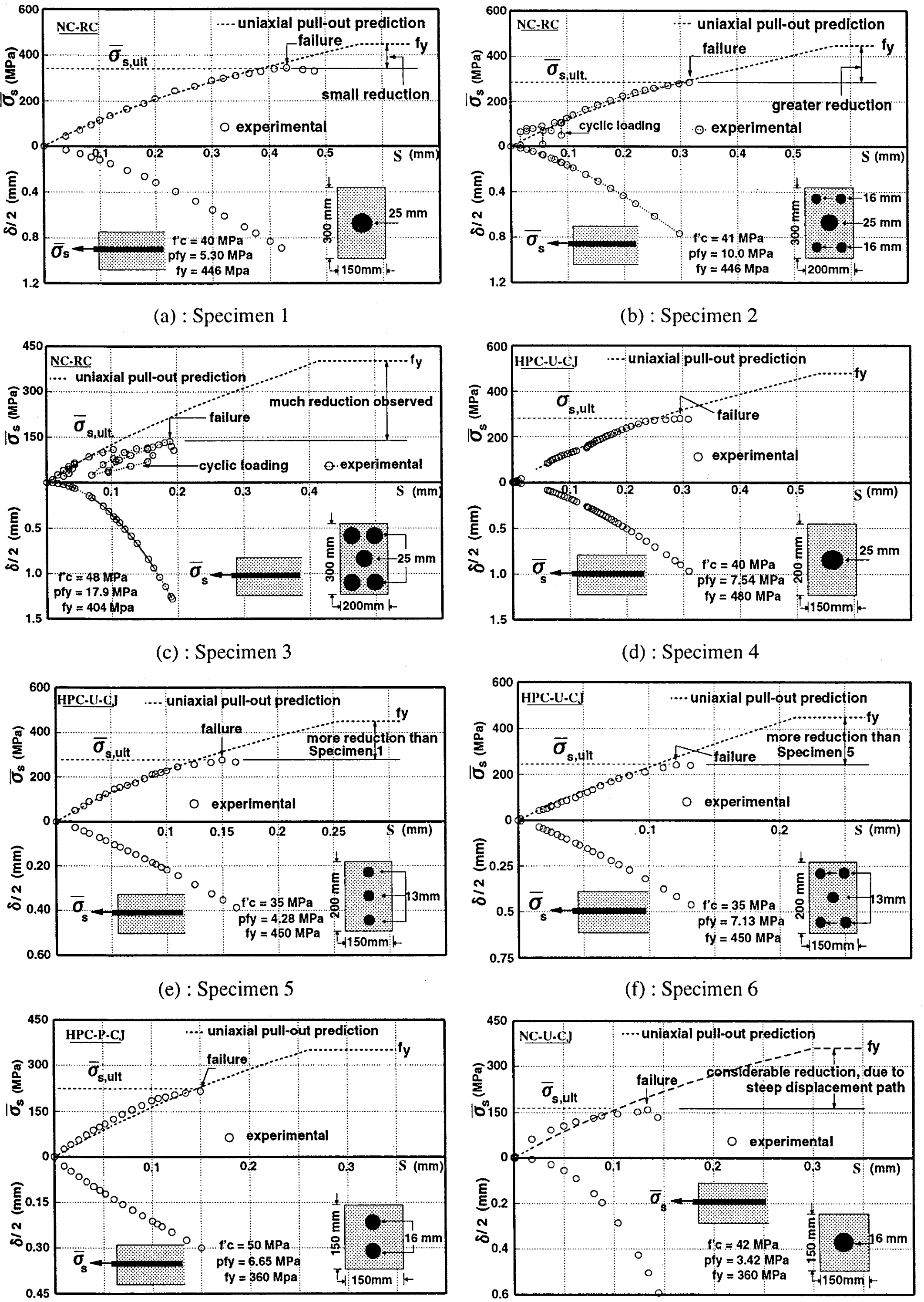

(a) : Specimen 1 (b) : Specimen 2

(c) : Specimen 3 (d) : Specimen 4

(e) : Specimen 5 (f) : Specimen 6

(g) : Specimen 7 (h) : Specimen 10

Fig.3 Mean axial stress at interface with associated axial pullout and transverse displacement, for rough cracks and construction joints

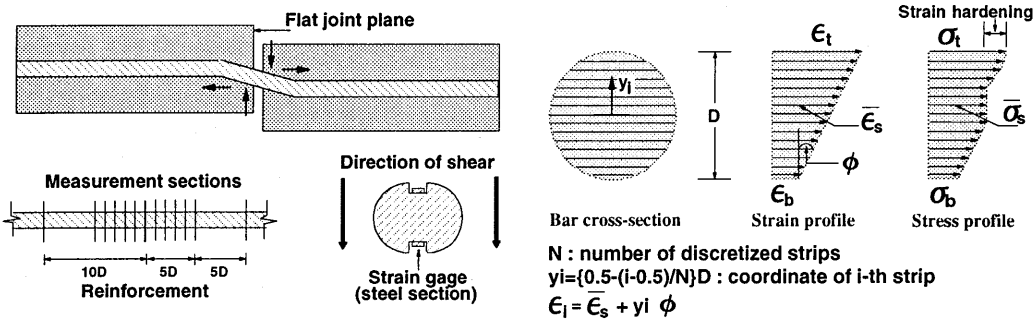

Fig.4 Discretization of reinforcing bars

bar from the joint plane up to a sufficient embedded length (defined as the control section) of up to 8 to 10 times the bar diameter; beyond this point the effects of crack shear displacement become negligible. The flat plane was obtained by concreting above an already hardened concrete block, with at least 24 hours left between concreting the two layers.

The relations between mean axial bar stress at the joint versus the pull-out at the joint, locally measured on the bar, and the associated transverse displacement of the bar, are shown in **Fig.3(d, e, f, and g),** along with similar results for rough cracks. It can be seen in **Fig.3** that, in the initial stages, the pullout behavior is close to the uniaxial case, but in most cases it deviates from this behavior as the transverse displacement rises. It is also clear that the axial capacity reached by the bar is less than the axial yield capacity, as determined from tests on bare steel bars under uniaxial loading[2].

The profiles of mean axial stress, mean axial strain, and induced curvature along the bar axis for typical specimens are shown in **Fig.5(a,b)**. The axial sectional mean strain, defined as ε_s,and the curvature $\phi(x)$ were obtained by measuring the local strains at top and bottom of the grooved section (ε_t, ε_b) at discrete intervals (See **Fig.4**).

$$\phi(x) = \frac{\varepsilon_t - \varepsilon_b}{D} \quad \bar{\varepsilon}_s(x) = \frac{\varepsilon_t + \varepsilon_b}{2} \tag{1}$$

where, D denotes the bar diameter.

The mean axial stress, which is sectionally averaged, is computed by assuming Euler-Kirchoff hypothesis (plane section remains plane) as,

$$\begin{aligned} \bar{\sigma}_s(x) &= \frac{1}{A_s}\int_{-D/2}^{+D/2} \sigma_s(\varepsilon_s)\,dA_s \\ \varepsilon_s(x,y) &= \bar{\varepsilon}_s(x) + \phi(x)\cdot y \end{aligned} \tag{2}$$

where, y is the local coordinate along the bar section, measured from the sectional centroid, and dAs is the y-derivative strip of the cross-sectional area along the bar section and As is the cross-sectional area.

The symbol σ_s denotes fiber stress and was obtained from the uniaxial stress-strain relation of the bar used as,

$$\begin{aligned} &\sigma_s = E_s \cdot \varepsilon_s \quad :0 < \varepsilon_s < \varepsilon_y \\ &\sigma_s = f_y \quad :\varepsilon_y \le \varepsilon_s < \varepsilon_{sh} \\ &\sigma_s = f_y\{1 - \exp(\varepsilon_{sh} - \varepsilon_u)/k\}\cdot(1.01 f_u - f_y) \\ &k = 0.047(400/f_y)^{2/3}, \quad \varepsilon_{sh} \le \varepsilon_s < \varepsilon_u \end{aligned} \tag{3}$$

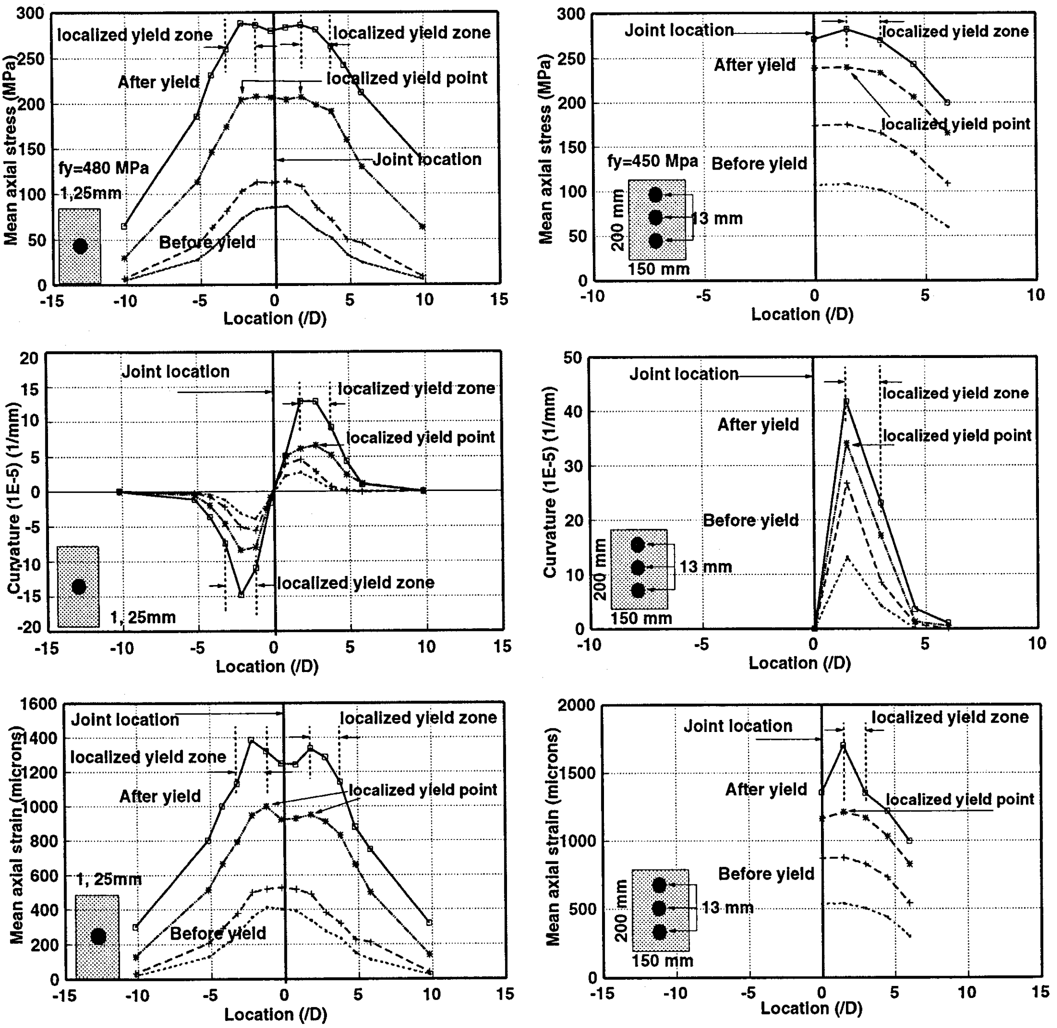

Specimen 4

Specimen 5

Fig.5(a) Profiles of mean axial stress, strain, and curvature along the reinforcing bar axis (Specimen 4 and 5)

where, f_y, f_u, ε_y and ε_u are the yield and tensile strength and corresponding strains, respectively, ε_{sh} is the strain at the onset of strain hardening and E_s is the initial elastic modulus of the bar. The numerical technique for solving the local axial stress from the local axial strain profile across a circular section, based on discretizing the bar section into a finite number of strips and using a predefined stress-strain relation for the bar, is shown in **Fig.4**.

In **Fig.3**, it can be seen that in the range where the axial stiffness is significantly reduced, the steel inside the concrete must have yielded to cause the non-linearity, in spite of the experimental determination that the crack section is still elastic. The mechanism by which this occurs can be understood from **Fig.5(a,b)**. The axial mean stress on the bar near the joint plane is quite smooth and relatively uniform very close to the crack, indicating loss of local bonding[2)].

But the profile for the axial mean strain is more complex, exhibiting local non-uniformities or 'jumps' near the joint plane, as shown in **Fig.5(a,b)**. The maximum strain in the bar occurs within the concrete at a location depending on the bar diameter, typically around 2D form the joint plane. The profile for the mean

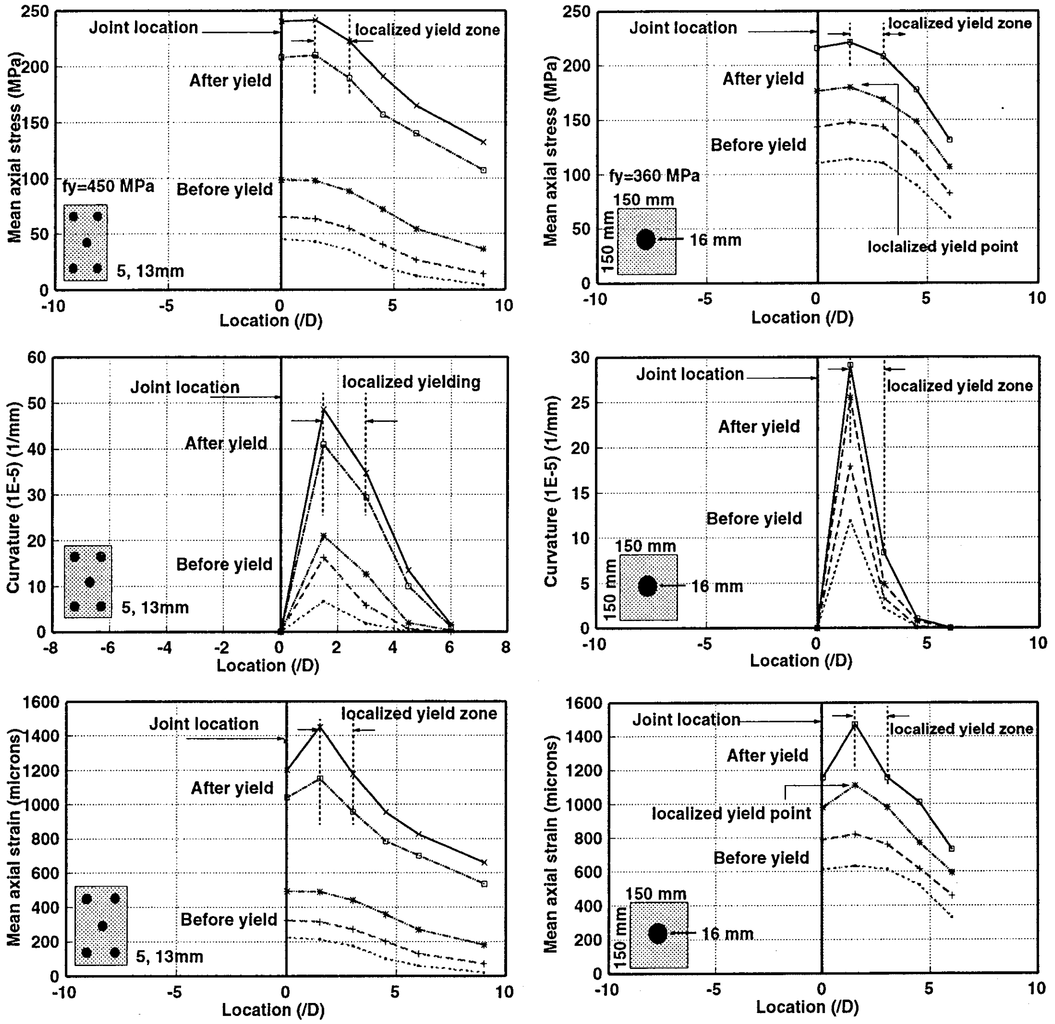

Specimen 6

Specimen 7

Fig.5(b) Profiles of mean axial stress, strain, and curvature along the reinforcing bar axis (Specimen 6 and 7)

axial strain follows the profile of local curvature experienced by the bar, which is also dependent on the bar diameter and is typically between 4D and 5D.

Here, with increasing transverse displacement, the length of the curvature profile increments slowly while maintaining a basically similar distribution profile. Since the integral of mean axial strain with respect to location along bar is equal to the pullout measured at the crack, the effect of the observed reduced axial stiffness on pullout can be attributed to this non-uniformity in mean axial strain.

In the experiments, strain measurements clearly demonstrated that localized yielding occurs in the extreme bar fibers within the concrete. However, the section at the interface remains fully elastic. The yield sections shown in **Fig.5(a,b)** indicate partial yielding of the bar cross-section and not complete yielding over the entire section. It is this partial yielding associated with local curvature which causes the loss of mechanical axial stiffness and the corresponding additional inelastic elongation along the axis.

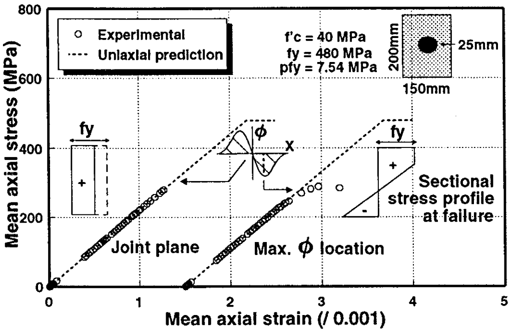

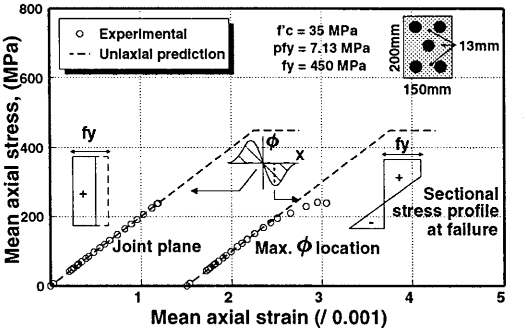

Fig.6 Sectionally averaged mean axial stress-strain relations at interface and maximum curvature location (upper : Specimen 4, lower : Specimen 6)

(2) Associated transverse shear and local yielding of reinforcing bars

The source of the internal plasticity is local curvature induced by the transverse displacement. The sectionally averaged mean axial stress-strain profile at the crack section and at the maximum curvature location, for some typical specimens, is shown in **Fig.6**. With a small crack opening and little transverse displacement, all fibers remain elastic at both locations. This corresponds to the initial part of the relations between steel stress at the crack versus pullout, since the mean axial stress-strain relation coincides with the constitutive law of a bare bar under uniaxial loading[7].

However, with increased transverse displacement, the curvature goes on increasing owing to deformational compatibility until the extreme fiber reaches the local yield strain. Qualitative local sectional stress profiles of the bar, at the ultimate shear capacity of the interface, are also shown in **Fig.6**.

This localized yielding causes the reduction in axial stiffness, as shown in **Fig.7**, which depicts the sectionally averaged mean stress-strain relation for a bar with bending -- represented by varying levels of constant curvature -- and axial force. Also shown in this figure is a general criterion for the failure condition of the bar under interactive stresses, expressed as a functional relationship in terms of ratios of actual forces to strength, under pure axial and bending forces.

The maximum possible interactive stress on the bar under such conditions, computed on the basis of the plane section theory of beams, is expressed by the interaction failure surface[16], defined by,

$$\left[\frac{P(x)}{P_o}\right]^2 + \left[\frac{M(x)}{M_o}\right] = 1 \tag{4}$$

where, $P(x)$ and $M(x)$ are the local axial force and bending moment along the bar axis, respectively, and P_o and M_o are the capacities under pure axial tension and bending. The derivation of such an equation requires knowledge of the stress-strain relationship of the material (which is idealized here as rigid-plastic), a definition of capacity in terms of limiting stress or strain (considered here as axial yield stress of the bar, f_y), and a solution to two equilibrium conditions for the given cross section: that is,

$$\begin{aligned} &\int_{-D/2}^{D/2} \sigma_s(x,y)\,dA_s(y) = P(x) \\ &\int_{-D/2}^{D/2} \sigma_s(x,y)\cdot y\cdot dA_s(y) = M(x) \end{aligned} \tag{5}$$

It is clear from **Fig.7** that the greater the curvature, or the bending moment producing the curvature, across the section, the greater is the reduction in axial stiffness. Also the maximum axial stress attained falls with increasing curvature. As seen in the test results, when an embedded bar is subjected to a coupled displacement path, the local maximum curvature does not remain constant but increases as the transverse

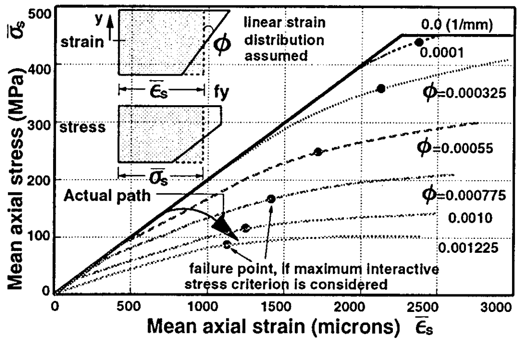

Fig.7 Effect of curvature on mean axial stress-strain relation of bar based on plane section theory

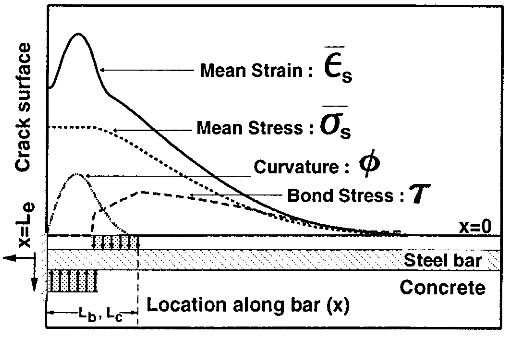

Fig.8 Schematic view of local state variables

displacement of the bar rises. Hence, the actual mean axial stress-strain path followed by the bar would be as shown by the arrow-headed line in **Fig.7**.

(3) Factors influencing localized yielding of steel

In the case of a heavily reinforced section or a smooth crack surface geometry, the transverse displacement associated with a corresponding bar pullout becomes higher, so as to satisfy the force equilibrium condition normal to the crack plane. A higher transverse displacement induces greater curvature, since compatibility requires that the double integral of the curvature profile equals the transverse bar displacement if the shear deformation is negligible. The higher curvature then results in reduced axial stiffness and also determines the maximum bar strength when subjected to simultaneous bending and axial forces. This is clear from the mean axial stress and curvature profiles for Specimens 5 and 6, which have the same bar diameter, as shown in **Fig.5(a,b)**. Specimen 6, which has a higher reinforcement ratio than Specimen 5, has a greater induced curvature and lower mean axial stress at failure.

Although the effect of increased reinforcement ratio on bar axial stiffness and strength is very significant, the effect of bar diameter is quite complicated. Several interactive parameters determine the overall effect of bar diameter on the reduction in axial stiffness and capacity of reinforcing bars at a crack or joint plane. This is because, although a bigger bar induces a higher transverse displacement to crack opening ratio as compared to a smaller-diameter bar, the relative magnitude of the maximum curvature of the former is smaller because it is distributed over a larger absolute length, which is also dependent on the bar diameter (typically 4D to 5D).

On the other hand, the effect of greater curvature on the smaller diameter bar is essentially lower on the extreme bar fibers because of the much smaller distance between the extreme fiber and the centroid of the bar section. This trend is clearly evidenced by comparing test results of maximum curvature and ultimate strength for Specimens 4 and 6, which have similar reinforcement ratios but different bar diameters, as depicted in **Fig.5(a,b)**. Overall, it can be said that the reduction in bar axial capacity is not highly sensitive to bar diameter. This is also verified by the test results, as shown in **Fig.3(d,f)**, where the reduction in axial strength for Specimens 4 and 6 is similar; these specimens have nearly the same reinforcement ratio and similar concrete strength, but different bar diameters.

(4) Mechanism of reduced axial stiffness caused by dowel action

Since the sectional mean stress-strain relation of a bar is affected by the curvature and the actually induced curvature is non-uniform, the resulting mean axial strain is complex, yet higher, no matter how smoothly the axial mean stress may vary. Since curvature at the crack location is zero due to geometric symmetry, pure axial tension is reproduced. But at other locations, the fiber strain is greater than the pure axial strain at the crack. Once the bar reaches its maximum axial sectional stress capacity at the critical maximum curvature location within the concrete, even when the section at the crack is still elastic, confinement by the bar is lost due to the total loss of stiffness, which is necessary to resist the bending associated with the transverse displacement.

It can be concluded that the curvature caused by the transverse shear initiates a localized inelastic axial strain which subsequently reduces the bar's mean yield strength and stiffness. This mechanism is the source of the reduced anchorage performance of embedded bars under a generic coupled displacement path consisting of axial pullout and transverse shear slip.

In modeling the reduced stiffness and strength of a bar under such a generic displacement path, simplified distribution profiles for the curvature and the deteriorated bond stress near the crack can be assumed, as shown in **Fig.8**.

4. DOWEL BEHAVIOR WITH COUPLED AXIAL PULLOUT

The capacity of an embedded bar to resist shear across its section, termed dowel action, may also be affected by the level of axial stress applied to the bar. Though the dowel force cannot be directly measured, it is possible to compute it using beam theory and profiles of induced curvature as,

$$V(x) = \frac{dM}{dx}, \quad M = E_s \cdot I_b \cdot \phi(x) \tag{6}$$

where, $M(x)$, $V(x)$ and $\phi(x)$ are the bending moment, shear force, and curvature along the bar axis, respectively, and E_s and I_b are the elastic modulus and moment of inertia of the bar section, respectively.

By fitting second-order polynomial functions to experimentally obtained curvature profiles (the method used to calculate local bond stress by Shima et al.[2]), the shear force at a crack point x=0 was computed. The computed shear stress ($\tau_s = V/A_s$) carried by the bar versus the associated bar transverse displacement, taken as one half of the interface plane displacement, and versus the sectionally averaged mean axial stress in the bar, are plotted in **Fig.9** for typical specimens.

The dowel shear stiffness rises linearly at first, and then there is a gradual loss of stiffness with increasing transverse displacement and mean axial stress. The ultimate shear carried by the bar at the peak shear capacity of the interface is about one third of the pure dowel capacity (170 MPa) for a bar of 25 mm diameter and in concrete of similar strength, but without any associated axial stress (as reported in reference (15)). This premature reduction in dowel stiffness and capacity, as compared to pure dowel performance, is brought about primarily by the coupled axial stress in the bar and also by the gradual softening of the concrete supporting the dowel due to the radial bond micro-cracks resulting from bar pullout, in addition to crushing of the concrete resulting from bar transverse displacement.

A comparison of the dowel performance of Specimens 5 and 6, whose parameters are all common except reinforcement ratio, clearly demonstrates the reduction in dowel capacity with increasing axial capacity (see **Fig.9(b,c)**). For Specimen 5, which has a lower reinforcement ratio, the associated displacement path in terms of ratio of axial pullout to transverse bar displacement is higher than for Specimen 6. Therefore, the maximum axial stress attained is higher, which reduces the dowel shear attained by Specimen 5 as compared to Specimen 6.

Theoretically speaking, if there is no transverse displacement and only axial pullout, the axial stress on the bar should reach the yield stress and dowel shear should be non-existent. Conversely, if there is no axial pullout and only transverse displacement, the axial stress should be zero and the full dowel capacity can be attained.

However, when there is a coupled displacement path, the pullout behavior is affected by the transverse shear, and the dowel action is in turn affected by the pullout. Thus pullout behavior and dowel behavior are mutually interactive and strongly influenced by the local plasticity that results from crack-steel interaction. The coupled displacement path brings about a reduction in both axial and transverse load carrying capacity of the bar, the ratio of which depends on the level of axial to transverse loading induced by the displacement path.

If the transverse displacement is high as compared to the axial pullout, the loss in axial capacity is greater because of the higher dowel shear attained. On the other hand, if pullout is comparatively higher, dowel capacity is lower due to the increased axial capacity attained as seen in **Fig.9(b,c)**.

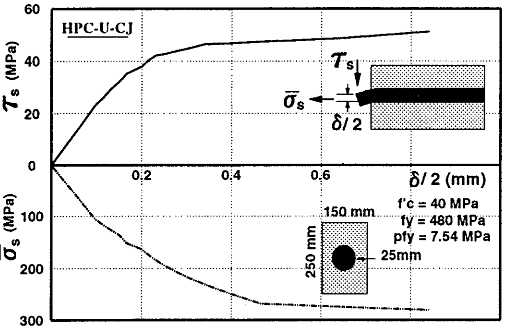

(a) Specimen 4

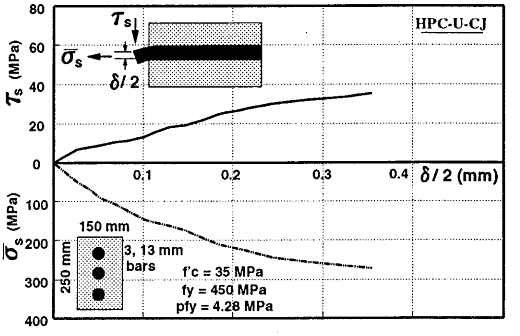

(b) Specimen 5

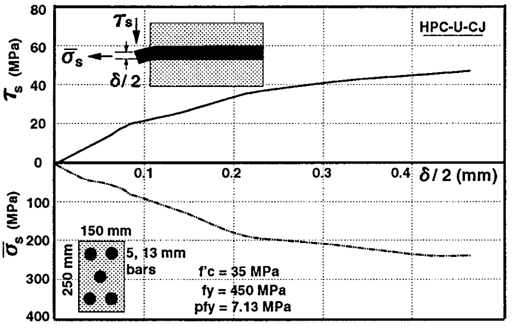

(c) Specimen 6

Fig.9 Shear stress and mean axial stress in bar versus transverse displacement

5. NONLINEAR INTERACTIONS WITH CRACK SHEAR IN CONCRETE

It has been reported by Mishima et al.[5] that when the reinforcement ratio exceeds 2%, the shear capacity of RC cracks and joints cannot be derived from a mere superposition of models for the stress transfer of plain concrete cracks and the one-dimensional pullout of reinforcement, even if they are verified independently. In general, analytical predictions of ultimate capacity exceed experimental results, even though such predictions neglect the dowel shear carried by the reinforcement.

From the experiments carried out in this study, it can be concluded that a primary reason for this reduced shear capacity may originate from the reduced confinement efficiency of the embedded bars against crack opening due to reduced axial capacity of the steel caused by shear slip along the crack. This in turn accelerates the loss in pullout stiffness and strength, finally determining the ultimate shear capacity. Mattock has also reported this failure mode in push-off tests[9] where the steel does not yield at the ultimate shear. But, the shear capacity is much less than that of a plain concrete crack[6] restrained by external confinement. It appears that shear failure is governed by failure of the concrete crack plane, whereas in reality it is the failure of steel within the concrete which initiates failure of the entire load-carrying system.

The relations between shear stress, shear slip, and surface crack opening along flat joint planes are shown for typical specimens in **Fig.10**. Also shown are analytical results as obtained by superposing the concrete stress transfer model by Bujadham et al.[3] and the bond pull-out model by Shima[2], which does not take into account local curvature of the steel and corresponding deteriorated anchorage performance. As this figure clearly shows, the shear capacity and associated deformational paths cannot be satisfactorily predicted by the above analysis. The highly over-predicted shear slip, lower surface crack opening, and higher shear capacity, despite neglecting the shear transferred by dowel action, is not substantiated by the test results.

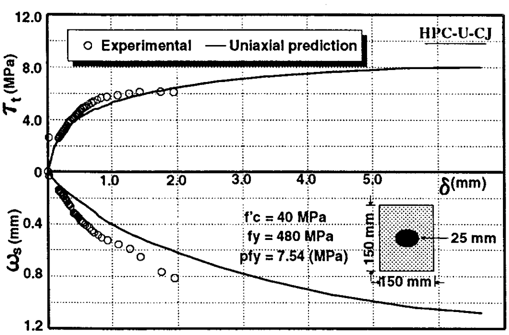

(a) Specimen 4

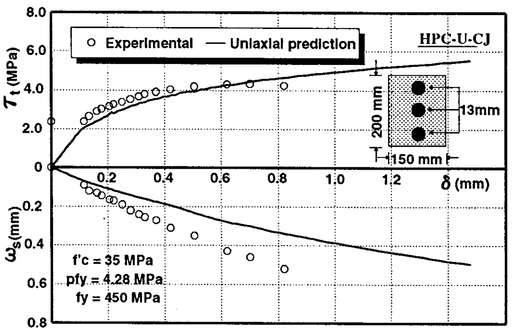

(b) Specimen 5

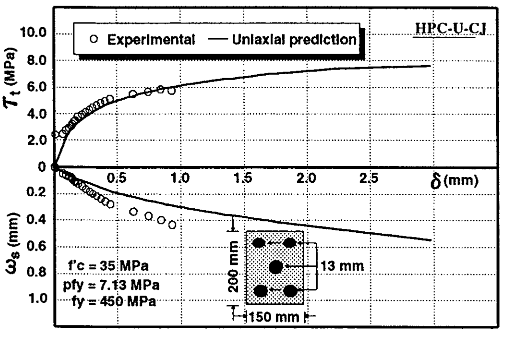

(c) Specimen 6

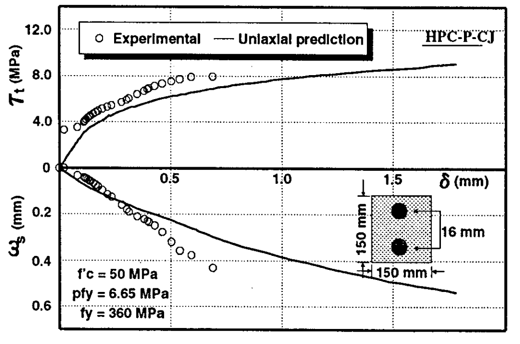

(d) Specimen 7

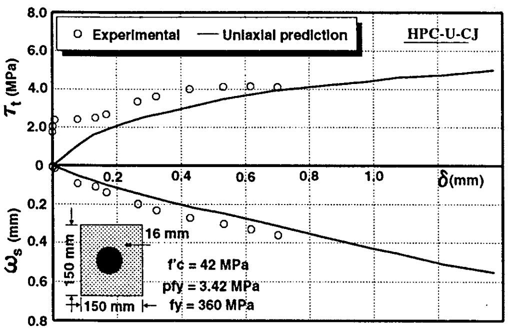

(e) Specimen 8

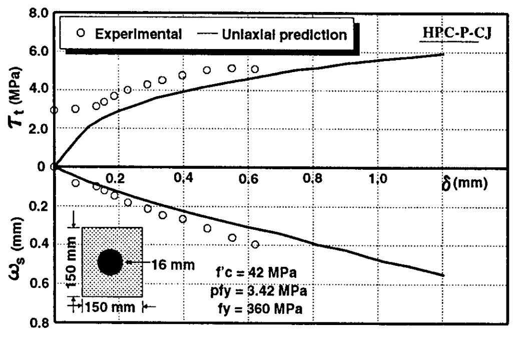

(f) Specimen 9

Fig.10 Comparison of analytical and experimental shear stress transferred with associated displacement paths at the interface for typical specimens

This lack of agreement between test and analysis may be explained by considering the reduced axial performance of a bar subjected to a coupled displacement path, as in the test, and that of one under axial loading as assumed in the analysis. The reduced bar performance would then be the major source of lower shear capacity and also one of the factors affecting the predicted and analytical surface crack opening (since the compatibility condition in the analysis assumes average crack opening to be twice the pullout).

It is verified in these experiments, that an increase in reinforcement ratio reduces the mean axial confining stress in the embedded bars.

However, an increase in reinforcement ratio increases the shear capacity, because the total confining force is higher with more reinforcement, and also the contribution to shear transfer by dowel action would also increase. If the reinforcement ratio is low, the discrepancy between analytical (simple superposition) and experimental results should be small, since the embedded bar would reach an axial stress close to its yield stress under pure axial tension and dowel shear, neglected in the analysis, would be small.

For larger reinforcement ratios, the over-estimation would be more significant. It is, however, worth noting that the dowel capacity would also increase with increasing reinforcement ratio, thereby balancing some of the change in total shear capacity. The true mechanism, in which the two modes of shear transfer (aggregate interlock and dowel action originating from the same displacement path defined at the interface) interact cannot be elucidated from the present analytical technique.

In view of this discussion, it is clear that by assuming the embedded bar provides an interface dilatancy resisting force equal to its yield capacity, and neglecting the shear force carried by the embedded bar, then regardless of the reinforcement ratio, material strengths, and interface geometry, a satisfactory prediction of interface capacity may be achieved in some cases. However, the true interactive behavior of steel and concrete is not modeled, and displacements associated with this capacity would as a consequence be inaccurate. Gross inaccuracies, even in predictions of capacity, would result under specific conditions. Therefore, for the accurate and versatile prediction of the shear capacity of different RC interfaces, it is imperative to develop a generalized model incorporating bar behavior under coupled displacement paths and plane concrete stress transfer behavior taking into account of interactions with the embedded bar.

6. CONCLUSIONS

The generic pullout behavior of deformed steel bars embedded in concrete and subjected to axial and transverse displacements was extracted from the overall mechanics of the reinforced crack section. Within the scope of this study, the following can be concluded:

(1) In addition to axial pullout of reinforcement due to crack dilatancy, transverse displacement at a crack plane induces a zone of curvature in the bar. Near the crack plane, the mean stress profile is uniform, but the mean strain profile exhibits significant non-uniformity due to the induced localized curvature.

(2) The induced curvature reduces the axial stiffness and strength of the reinforcement within the concrete as a result of local inelasticity arising in the bar within the concrete.

(3) The reduced axial stiffness of the reinforcement causes an inelastic axial strain along the bar under lower axial stress. This local inelasticity gives rise to greater pullout and loss of anchorage performance.

(4) The reduced stiffness and strength of the confining reinforcement affects the shear capacity of the rough surfaces of the concrete interface. The degree of reduction is chiefly related to the displacement path to which the bar is subjected at the interface.

(5) The dowel behavior and pullout behavior of embedded bars are mutually interactive and interdependent. The pullout behavior is affected by the transverse shear, and the dowel action is in turn affected by the pullout behavior. This mutual dependence is strongly influenced by the local plasticity resulting from the interaction between the interface and the embedded bar.

(6) In order to propose a versatile model for predicting the stress transfer behavior of an RC interface, it is crucial to formulate a model for the reduced axial stiffness and strength of an embedded bar under the coupled effect of axial pullout and transverse displacement.

In our next study, we will attempt to formulate such a generic bar model.

REFERENCES

1) Okamura, H., and Maekawa, K.: Nonlinear analysis and constitutive models of reinforced concrete, Giho-do Press, Tokyo, 1991

2) Shima, H., Chou, L., and Okamura, H.: Micro and macro model for bond behavior in reinforced concrete, Journal of the faculty of engineering, The University of Tokyo (B), Vol. 39, No.2, 1987

3) Bujadham, B., Maekawa, K., and Mishima, T.: Cyclic discrete modeling for reinforced concrete, Computer aided analysis and design of concrete structures, Pineridge Press, 1990, pp.1225-1236

4) Mishima, T., Yamada, K., and Maekawa, K.: Localized deformational behavior of a crack in RC plates subjected to reversed cyclic loads, Proc. of JSCE, No.442/V.-16, Feb., 1992, pp.161-170

5) Mishima, T., Bujadham, B., and Maekawa, K.: A development of a RC discrete crack model under reversed cyclic loads and a verification of its applicable range, Proc. of JSCE, No.442/V.-16, Feb., 1992, pp.181-190

6) Li, B., Maekawa, K., and Okamura, H.: Contact density model for stress transfer across cracks in concrete, Journal of the faculty of engineering, The University of Tokyo (B), Vol. 40, No.1, 1989

7) Mishima, T., Bujadham, B., Maekawa, K., and Okamura, H.: A development of constituent material models for a reinforced concrete discrete crack, Proc. of JSCE, No.442/V.-16, Feb., 1992, pp.171-179

8) Bartos, P. (editor): Bond in Concrete, Applied Science Publishers, London, 1982

9) Mattock, A. H., and Hawkins, N. M.: Shear transfer in reinforced concrete-recent research, Journal of PCI, Vol.17, No.2, March-April, 1972

10) Mishima, T., Yamada, K., and Maekawa, K.: Discrete crack finite element analysis of reinforced concrete structures subjected to alternate force and thermal load, Proc. of JSCE, No.442/V-16, Feb.,1992, pp.201-210

11) Bujadham, B., and Maekawa, K.: The Universal Model for Stress Transfer across Cracks in Concrete, Proceedings of the JSCE, No. 451/V-17, pp.277-287, 1992

12) Bujadham, B., and Maekawa, K.: Qualitative Studies on Mechanisms of Stress Transfer across Cracks in Concrete, Proceedings of the JSCE, No. 451/V-17, pp.265-275, 1992

13) Maekawa, K., Khan, J., Qureshi, J., and Mishima, T.: Reduced Axial Stiffness of Deformed Bars Under Shear Slip along a Crack in Concrete, Bond in Concrete, CEB, Latvia, Oct. 1992

14) Yamada, K., and Aoyagi, Y.: Shear Transfer along Cracks, Proceedings of the JCI 2nd Colloquium on Analytical Studies on Shear Design of Reinforced Concrete Structures, JCI, pp. 19-26, Oct. 1986

15) Poli, S. D., Prisco, M. D., and Gambarova, P. G.: Shear Response, Deformations, and Subgrade Stiffness of a Dowel Bar Embedded in Concrete, ACI Structural Journal, V. 89, No. 6, 1992, pp. 665-675

16) Beedle, S. L., Ready, J. A., and Johnston, B. G.: Tests of Columns under Combined Thrust and Moment, Proc. of Society of Experimental Stress Analysis, Vol.8, 1950, pp.109-132